On Geopotential Data and Ellipticity of the Balance Equation: A Data Study

JAN PAEGLE AND JULIA N. PAEGLE

Department of Meteorology, University of Utah, Salt Lake City 84112

(Manuscript received 21 September 1975, in revised form 12 July 1976)

ABSTRACT

One year of geopotential data obtained from the National Meteorological Center and the National Center for Atmospheric Research are diagnosed for the occurrence of non-elliptic regions with respect to the balance equation. The highest frequencies of such occurrences appear at 200 mb over the subtropical oceans where there are few radiosonde observations. Substantial 200 mb frequencies are also found over the United States in the summer season above a reliable data net. A diagnosis of flow divergence implied for the non-elliptic data by a theoretical analysis of Paegle and Paegle (1974) produces values greatly in excess of typical observations. This suggests that the gridding of the data by objective analysis may not have been adequate and/or that the aforementioned theory overestimates flow divergence in these regions. It is likely that non-elliptic data are important for initialization of primitive equation forecast models. It may be inferred that greater data accuracy, as well as better initialization techniques within non-elliptic regions, are required.

1. Introduction

A consistent initial balance of the mass and wind fields is important for successful short-range forecasting with the primitive equations. The simplest initialization technique is based upon the geostrophic assumption. This has been used quite commonly (e.g., Washington and Baumhefner, 1975), although it represents the lowest order balance of the equations of motion. The next order of balance is described by the balance equation (Charney, 1955; Miyakoda, 1956; Shuman, 1957). This has not been used as extensively as might be expected for three reasons. First, the ellipticity condition for its solution (Houghton, 1968) sometimes requires large initial pressure data modification in the upper troposphere (Cressman, 1959; Ellsaesser, 1968). Second, it is more time consuming and this may be important for operational application. Finally, it does not appear to produce more accurate winds than simpler relationships (Ellsaesser, 1968).

The geostrophic and balance wind fields are both essentially solenoidal, although slight divergence occurs with the geostrophic wind (Washington and Baumhefner, 1975). A correct simulation of the initial divergence field should also be important because baroclinic energy conversions are absent initially if the flow is nondivergent. It is therefore somewhat surprising that forecasts appear rather insensitive to the initial divergent velocity component obtained from a quasi-geostrophic formulation (Houghton *et al.*, 1971).

The scale analysis and perturbation expansion which justify consistency of various orders of approximation (geostrophic, quasi-geostrophic divergent, balanced, etc.) may be questionable when the ordering expansion parameter (the Rossby number) has magnitude 1. This is the case in deep cyclones and strong anticyclones where the relative vorticity has the same magnitude as the Coriolis parameter.

The case of strong anticyclones is particularly troublesome because the geostrophic relative vorticity may be only about half the actual relative vorticity, and the balance equation may yield no solution unless the pressure data are modified. An alternative to pressure modification has been suggested by Paegle and Paegle (1974; hereafter referred to as I). In this alternative divergent flow accelerations balance that portion of the divergent pressure force field which cannot be balanced by centripetal and Coriolis effects. Thus, a directly forced divergent flow results which may be much larger than the indirect "compatibility" divergent flow obtained through the omega equation.

The existence of strongly divergent upper tropospheric anticyclones has been documented above the monsoon by Krishnamurti (1971) and above severe weather events by MacDonald (1976). MacDonald's case studies were performed over areas of good data coverage, were associated with pressure patterns for which the balance equation is not elliptic, and they exhibited abnormally large flow divergence.

The purpose of this paper is to describe the occurrence of such non-elliptic pressure data in the National Meteorological Center (NMC) analyses. This is important because many primitive equation forecasts are

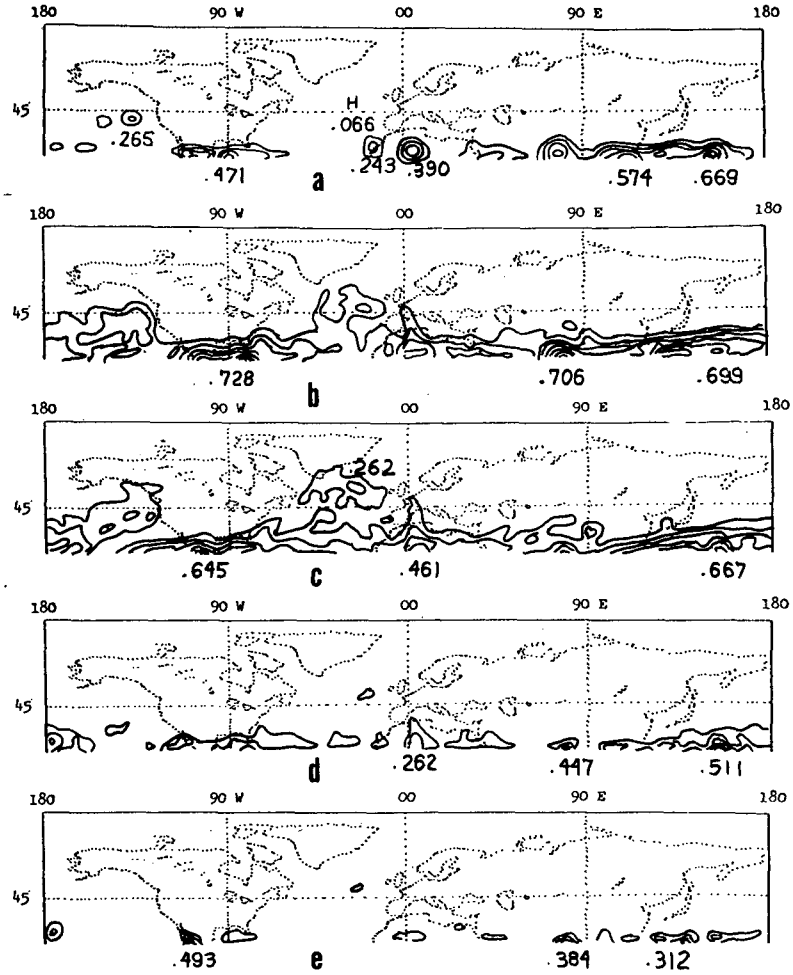

FIG. 1. Percentage occurrence of non-elliptic geopotential data for March, April, May 1970 (spring) at (a) 100 mb, (b) 200 mb, (c) 300 mb, (d) 500 mb, (e) 700 mb (normalized to 100%). Isopleth interval is 10%.

initialized with these data. It is likely that many of these occurrences are a consequence of poor data coverage and inadequate objective analysis techniques. In any event, they are a problem for initialization because the seasonal frequency of non-elliptic data in some locations at 200 mb is as high as 80%. Such frequencies are discussed in Section 2. Section 3 displays characteristics of the divergent velocity field that would ensue on the assumption that the velocity field adjusts to the mass field as suggested in I. Section 4 summarizes conclusions.

2. Frequencies of non-elliptic data

a. Data

Geopotential heights archived by Jenne (1975) at the National Center for Atmospheric Research (NCAR) comprise the data basis of this investigation. Objective analysis of this data set was performed by the National Meteorological Center with techniques described by Cressman (1959) and McDonnell (1962, 1967). The data were obtained on a $2\frac{1}{2}$ latitude-longitude spherical grid poleward of 20°N.

A year of data beginning 1 June 1969 was selected. Statistics were not computed for other years. However, examination of some other dates in spring and summer of 1967, 1968, 1969, and spring 1974 suggest that the structure and preferred regions of occurrence of non-elliptic geopotential data were similar to those of the year described in the present research.

b. Ellipticity

The balance equation is non-elliptic when

$$f^2+2\nabla^2\Phi+2\beta u<0 \qquad (1)$$

(Houghton, 1968). Here Φ represents the geopotential of a constant pressure surface, f is the Coriolis parameter, β the meridional gradient of f, and u is the zonal flow component. When condition (1) is satisfied, a measure of the non-ellipticity is given by

$$f^2+2\nabla^2\Phi+2\beta u. \qquad (2)$$

In principle it is impossible to compute this, because u can be obtained only after solution of the flow field, and this cannot be done for non-elliptic cases. In practice u can be approximated by a geostrophic value.

The non-ellipticity criterion we used refers to the slightly modified version of the balance equation described in I. The divergence field given by this approach for non-elliptic cases is a realizable steady-state limit of a set of time-dependent equations (Paegle and Paegle, 1976; hereafter referred to as II). For a given geopotential field the same divergence and vorticity fields result for all flow boundary conditions. The customary balance equation can also be made elliptic by introducing sufficient divergence instead of modifying the pressure field. However, in this case neither the resulting divergence nor the vorticity are unique functions of Φ because of the dependence of the solution kinematics on unknown boundary conditions. These points are discussed in I, which also gives formulas for the ellipticity condition and the divergence that results from non-elliptic data in a Cartesian geometry.

In the case of spherical geometry it is necessary to approximate metrical terms using geostrophic values. The non-ellipticity criterion that is suggested in I then becomes

$$(f^2+\nabla^2\Phi-G)-|f[(\nabla^2\Phi-G)^2/f^2-(A_g^2+B_g^2)]^{\frac{1}{2}}|<0, \quad (3)$$

where

$$G=-\beta u_g-(v_g^2+u_g^2)/a^2-(2\tan\phi/a^2)\left[u_g\frac{\partial u_g}{\partial\phi}+v_g\frac{\partial v_g}{\partial\phi}+\left(u_g\frac{\partial v_g}{\partial\lambda}-v_g\frac{\partial u_g}{\partial\lambda}\right)\Big/\cos\phi\right], \quad (4)$$

$$A_g=-\left\{\frac{\partial}{\partial\phi}[(u_g^2+v_g^2)\sin\phi/a]+2\frac{\partial}{\partial\lambda}(u_gv_g\tan\phi/a)\right\}\Big/(af\cos\phi)-\left\{\frac{\partial}{\partial\phi}\left(\frac{1}{a}\frac{\partial\Phi}{\partial\phi}\cos\phi\right)-\frac{\partial}{\partial\lambda}\left[\frac{\partial\Phi}{\partial\lambda}\Big/(a\cos\phi)\right]\right\}\Big/(af\cos\phi)-\beta u_g, \quad (5)$$

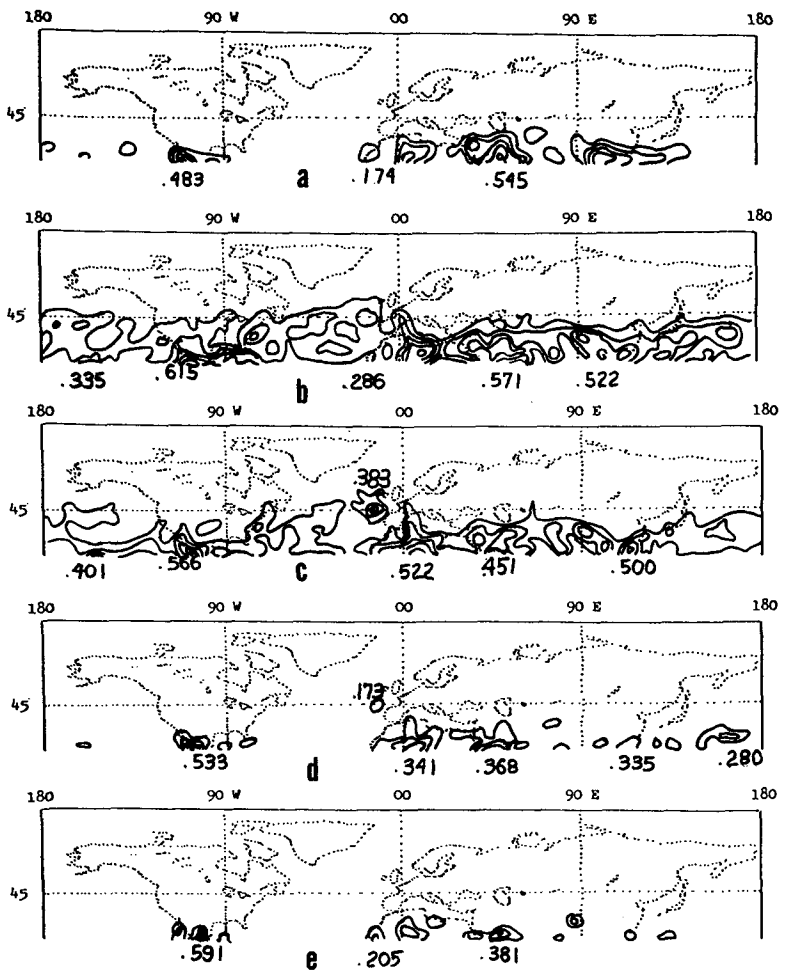

FIG. 2. As in Fig. 1 except for June, July, August 1969 (summer).

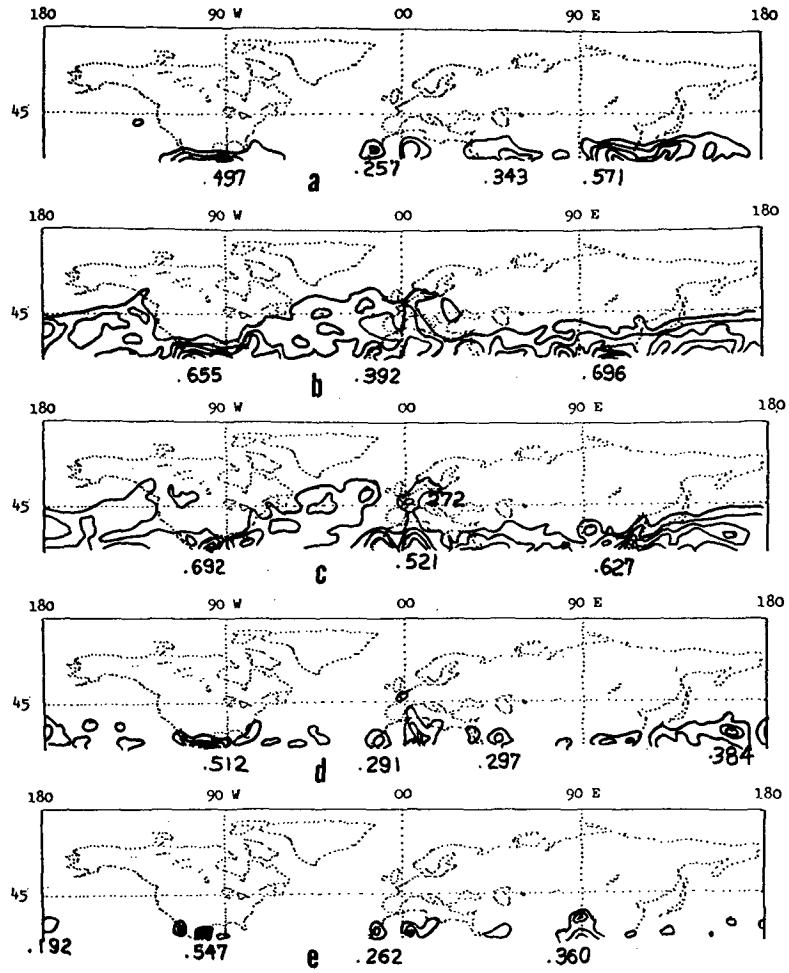

FIG. 3. As in Fig. 1 except for September, October, November 1969 (autumn).

$$B_g=\left\{-\beta v_g+4u_g\frac{\partial u_g}{\partial\lambda}\tan\phi/(a^2\cos\phi)\right.$$
$$\left.-\left[\frac{\partial}{\partial\lambda}\left(\frac{\partial\Phi}{\partial\phi}\right)+\frac{\partial}{\partial\phi}\left(\frac{\partial\Phi}{\partial\lambda}\right)\right]\Big/(a^2\cos\phi)\right\}\Big/f, \quad (6)$$

u_g and v_g are zonal and meridional geostrophic flow components, respectively; ϕ and λ are latitude and longitude, respectively; and a is the radius of the earth.

Eq. (3) corresponds to (32) of I with the introduction of geostrophic values for the metrical terms that are needed in Eqs. (25)–(28) of I for application on a sphere. The metrical terms were included principally for completeness, as they have little quantitative effect on our statistics, except within a few grid points of the pole. The dominant term in G is βu_g which has a typical magnitude of 10^{-10} s^{-2}. The dominant terms in A_g and B_g are those resulting from geostrophic deformation rates, and have typical magnitudes of 10^{-5} s^{-1}. Inspection of (3), (4), (5) and (6) then reveals that (1) can usually be satisfied for smaller magnitudes of $\nabla^2\Phi$ than (3). Consequently, the customary balance equation would be non-elliptic more frequently than indicated by criterion (3), and non-ellipticity frequencies presented in this section are probably underestimates for criterion (1).

The divergence D suggested in I for the non-elliptic cases is

$$D=\{-(f^2+\nabla^2\Phi-G)+|f[(\nabla^2\Phi-G)^2/f^2-(A_g^2+B_g^2)]^{\frac{1}{2}}|\}^{\frac{1}{2}}. \quad (7)$$

For the elliptic cases a steady non-divergent flow is possible, and divergence was not computed in that case.

If the radical in (3) is negative, the following approximations are used instead of (3):

$$f^2+2\nabla^2\Phi-2G+A_g^2+B_g^2<0, \quad (8)$$

$$D=\{-(f^2+2\nabla^2\Phi-2G+A_g^2+B_g^2)\}^{\frac{1}{2}}. \quad (9)$$

These are reasonable when $D^2/f^2\ll 1$.

A negative radical in (3) can arise together with condition (8) in those cases when the geostrophic shear and curvature vorticity are of opposite sign,

and the total geostrophic vorticity is sufficiently anticyclonic to satisfy the non-ellipticity condition. This situation did not occur in any of the individual cases that we examined subjectively, and probably constitutes only a small fraction of the total non-elliptic cases.

Evaluation of (3)–(9) was done by standard centered differencing approximations using a $2\frac{1}{2}°$ grid.

Figs. 1–4 present the frequencies with which the non-elliptic criterion (3) or (8) was satisfied at various levels for spring, summer, autumn and winter. The highest frequencies are in the subtropics at all levels and seasons, and at 200 mb at all seasons and geographical locations. Thus, the typical non-elliptic anticyclone appears to be warm core below 200 mb and cold core above this level, and is most commonly found in the subtropics.

The largest frequency (86.4%) is found in winter within the subtropical Pacific at 200 mb. The largest frequency we found in a data-rich zone (21%) occurred in summer and was centered at 100°W, 32.5°N over the southern United States. Thus, while many cases cannot be substantiated by a dense data net, a substantial fraction persists in regions where upper level data density is commensurate with current NMC grid spacing.

Fig. 5 presents the average value of D as given by (7) and (9) for the four seasons at 200 mb. Here D is the divergence field suggested in I as well as a measure of the average intensity of the non-elliptic high-pressure regions. The largest average values exceed 0.3×10^{-4} s^{-1}, and are about an order of magnitude greater than the 200 mb kinematically computed divergences of Krishnamurti (1971). Individual cases have central D values ranging from 0.2×10^{-4} to 0.6×10^{-4} s^{-1}, but rarely exceeding 0.9×10^{-4} s^{-1}.

c. *Error sources*

The two most important sources of error in our results are data errors (particularly over oceans) and simplifications in the divergence-geopotential relationship derived in I.

The NMC objective analysis scheme weights wind

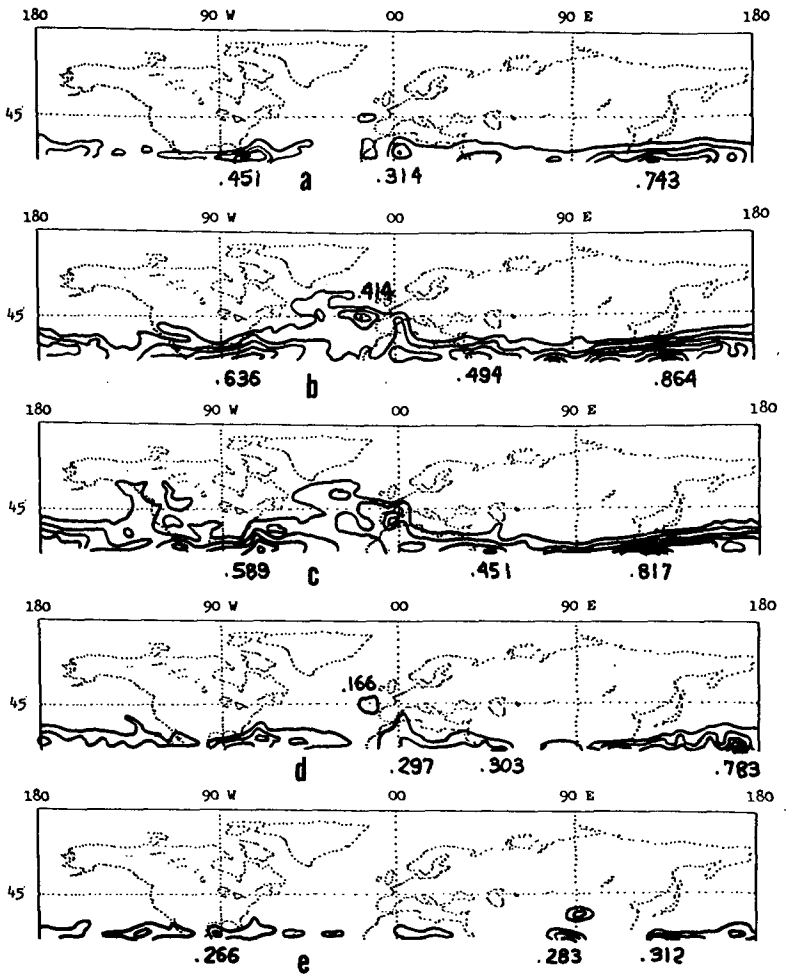

FIG. 4. As in Fig. 1 except for December 1969, January, February 1970 (winter).

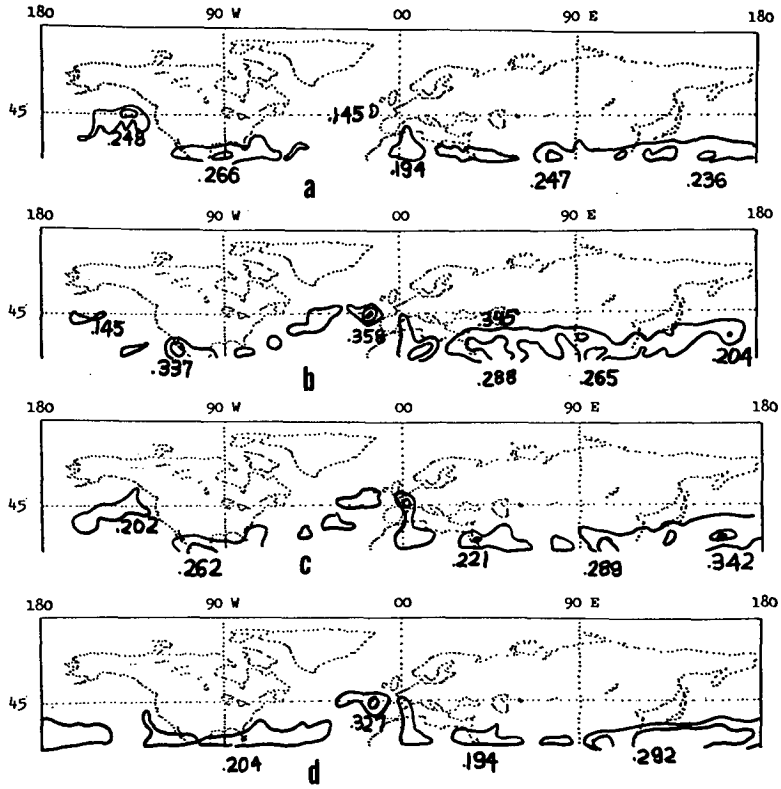

FIG. 5. Average value of D (see text) at 200 mb for (a) spring, (b) summer, (c) autumn, (d) winter. Each unit represents 10^{-6} s^{-1} and the analysis interval is 10^{-5} s^{-1}.

data more heavily than geopotential data in determination of the geopotential gradients (Cressman, 1959). In a region of dense data coverage, the actual geopotential gradients may persist in the data tabulations, but in locations with few data points the analyzed gradients may be more nearly geostrophic. For a given flow strength the geostrophic assumption generally overestimates the height gradients in an anticyclonic system and might tend to falsely produce "non-elliptic" geopotential fields. This may partially explain the high frequencies over the data voids of subtropical oceans.

Assuming that a high pressure region is non-elliptic, it may nonetheless fail to exhibit the theoretical flow divergence proposed in I because of various simplifications in that theory. The steady-state assumption may not be sufficiently well satisfied, neglect of higher order flow derivatives may not be justified, and omission of vertical structure effects (stratification) may be critical. Some of these questions are discussed in II.

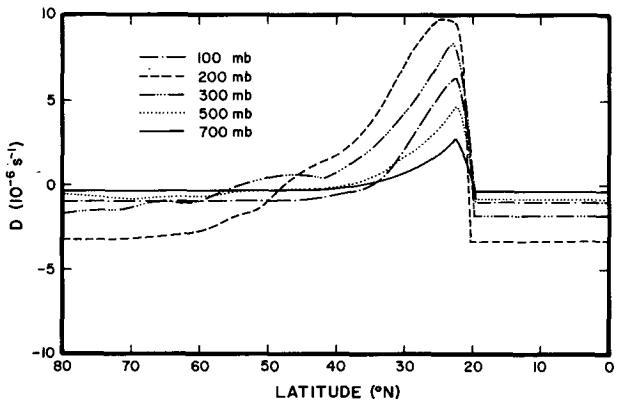

FIG. 6. Average value of D for June 1969–May 1970 as a function of latitude and level.

3. Divergent velocity fields

Divergent velocity components can be computed from the divergence diagnosed by (7) or (9). Since these fields have no convergence, there is a net mass source at any pressure level that has some non-elliptic geopotential data. To avoid this unrealistic situation, we arbitrarily and uniformly added the value of divergence at each elliptic point that would be necessary to produce zero net divergence over the Northern Hemisphere. This was done in a region from the equator to the pole, in each case including the region from the equator to 20°N. The resulting divergence averaged over longitude and the year of data is shown as a function of level and latitude in Fig. 6. It peaks strongly at 200 mb and 25°N.

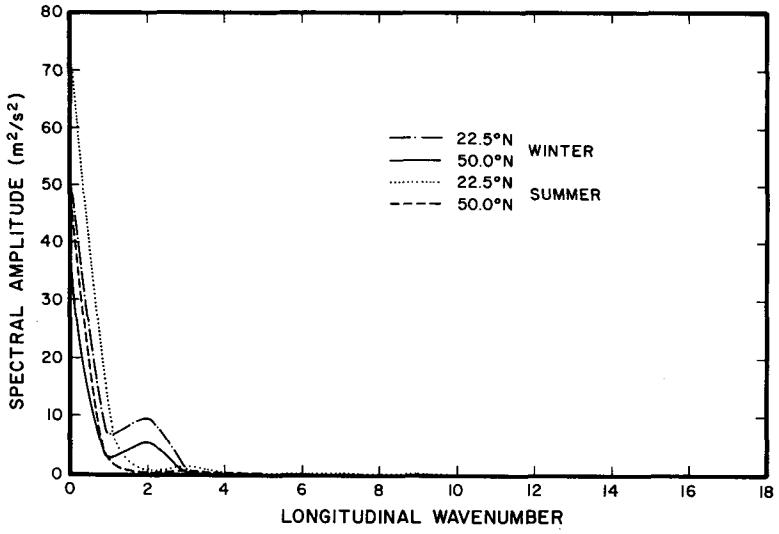

FIG. 7. Longitudinal spectra of meridional wind component: dotted curve, 50°N, winter; dashed curve, 22.5°N, winter; solid curve, 50°N, summer; dash-dotted curve, 22.5°N, summer.

The following equation was solved for the velocity potential χ over the Northern Hemisphere for each case:

$$\nabla^2\chi = D. \tag{10}$$

Here D is the divergence given by (7) or (9) at non-elliptic grid points, and by the compensating value described in the previous paragraph at other grid points. The solution of (10) was accomplished numerically through programs and techniques developed by Swartztrauber (see Adams *et al.*, 1975), using $\chi = 0$ at the equator as the boundary condition. Tests to determine the sensitivity of our results to the boundary conditions and compensating convergence are described in the Appendix.

The divergent velocity components were computed from

$$u = \frac{\partial\chi}{\partial\lambda} \Big/ (a\cos\phi), \quad v = \frac{\partial\chi}{\partial\phi} \Big/ a. \tag{11}$$

Some 200 mb longitudinal spectra of the meridional velocity components are displayed in Fig. 7. These spectra were obtained by averaging the spectra of individual observations over a whole season. Almost all of the variance is present at wavenumbers >3. Although the divergence is much weaker at 50°N than at 22.5°N, the higher latitude exhibits almost as much amplitude in v as the lower latitude in the

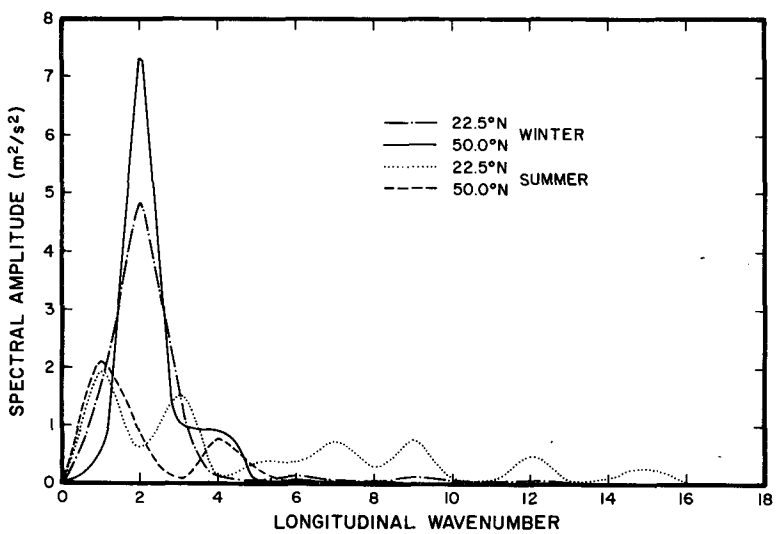

FIG. 8. As in Fig. 7 except for zonal wind component.

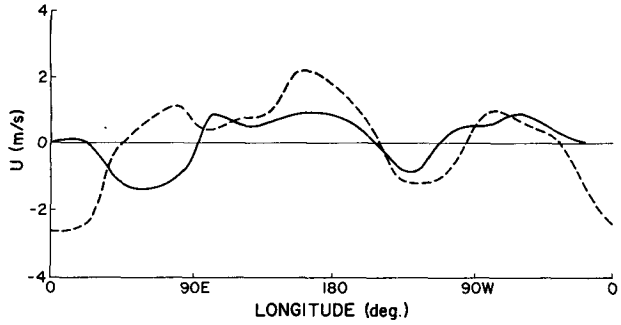

FIG. 9. 200 mb divergent zonal wind component. The solid curve, taken from Krishnamurti *et al.* (1973), represents the observed divergent zonal component for summer 1967, averaged from the equator to 30°N. The dashed curve is the value at 22.5°N diagnosed from the non-elliptic pressure fields, summed over wavenumbers 0, 1, 2, 3 for summer 1969.

average and in wavenumber 1, and there is more amplitude in wavenumber 2 at 50°N than at 22.5°N.

Zonal flow spectra (Fig. 8) have zero mean and are somewhat flatter than meridional spectra, particularly in the summer at 22.5°N. However, most of the variance is again present in the first four waves.

Thus, while the non-elliptic regions tend to be confined to the subtropics, are rather patchy and produce almost flat spectra for the variance of D (not shown), divergent velocity components appear to be induced most strongly in the long waves and at all latitudes.

The divergent flow contributions summed over the lowest four wavenumbers are displayed for 22.5°N in Figs. 9 and 10. Summertime tropical observations of Krishnamurti *et al.* (1973) and Sadler (1975) are included for reference.

If non-ellipticity were important for divergence, some agreement might be expected in the trends of these curves, since the major sources of observed summer divergent motions are contained in the centers of activity located over the subcontinent of Asia, the Sahara and northern Mexico. NMC data coverage might be adequate in these regions.

The longitudinal trends in the diagnosed motion fields are similar to the observations in the region to the west of Greenwich, across the dateline to about 100°E. The diagnosed divergence field contains a strong mass source centered at about 50°E, 30°N which has no counterpart in the data of Krishnamurti *et al.* (1973) or Sadler (1975). This produces large discrepancies in the curves from Greenwich eastward to about 90°E.

Although the diagnosed flow variation with longitude appears to agree with broad features of the tropical data over much of the globe, there are local discrepancies. Some disagreement may be expected because of the different periods of the data sets, the different latitudes considered, and our arbitrary convergent compensation and boundary conditions. Moreover, Sadler's meridional wind includes rotational as well as divergent flow (although his longitudinal mean of almost 5 m s^{-1} must be purely divergent). Thus, pointwise comparisons are not meaningful.

However, it is pertinent to point out that the diagnosis and Sadler's (1975) observations each suggest a mean Hadley cell with a 200 mb strength of at least 5 m s^{-1}. Furthermore, data of Krishnamurti *et al.* (1973) and our diagnoses both indicate east-west overturning with magnitude at least 1 m s^{-1}.

While the diagnosed fields have peaks which are about twice as strong as these observations, they are not larger by an order of magnitude, as might have been expected from the large diagnosed divergence fields. Therefore, while it is highly speculative to conjecture that non-elliptic pressure fields have significant impact upon the Hadley cell and large-scale east-west overturning, the possibility is supported by this investigation, and this warrants further study.

4. Conclusions

Virtually every hemispheric 200 mb chart that we examined visually exhibited non-elliptic geopotential data at some points. Undoubtedly many of the non-elliptic cases are a result of inadequate data coverage and objective analysis techniques that use the geostrophic assumption to fill gaps in geopotential data. However, these are also cases that cannot be discounted on this basis and which would not be eliminated by reasonable changes of the analysis technique. At this point it is difficult to estimate the true percentage of non-elliptic data.

Such data present a dilemma for primitive equation model initialization. Geostrophic initialization would develop extra divergence in the first hours of adjustment, as described in II. If the divergence field adjusts

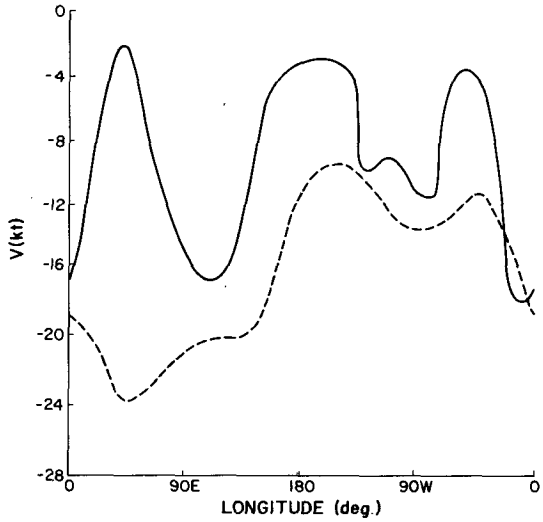

FIG. 10. 200 mb meridional wind components. The solid curve is taken from Sadler (1975) and represents the observed equatorial August average for a number of years. It includes divergent and rotational contributions. The dashed curve (diagnosed as in Fig. 9) represents the divergent contribution only.

to the mass field as indicated, then divergence would locally be an order of magnitude larger than typically expected. The long-wave flow field, the Hadley and Ferrel cells, and east-west large-scale circulations would also be significantly affected, with larger magnitude and locally different phasing than is indicated by kinematically computed divergence fields. These facts suggest that the non-ellipticity is not as pronounced in reality as in the data set or that the adjustment described in I is not generally observed. However, there is increasing evidence that the latter is not the case, as discussed in II.

The non-elliptic regions of the best extended data set that is currently available have major ramifications for the evolution of large-scale flow. It follows that a careful examination of non-elliptic height data over dense data regions could be instructive, and that correct initialization in such regions may be particularly important for prediction by primitive equation models.

Acknowledgments. Most of this research was accomplished while we were visitors at the National Center for Atmospheric Research which is sponsored by the National Science Foundation. The computations were performed on the NCAR computers, and the data were obtained through Roy Jenne. Partial support for this research was provided through NSF Atmospheric Sciences Section Grant GA-40387.

APPENDIX

Sensitivity to Boundary Conditions

The divergent flows described in Section 3 depend upon boundary conditions imposed on χ at the equator. We have solved the inhomogeneous Dirichlet problem with homogeneous boundary conditions

$$\nabla^2\chi=0,\ \chi=0,\ \text{on the equator.}$$

If χ were not zero on the equator, or if a Neumann problem is solved, then the modification to our solution would be given by the solution of the homogeneous problem with the appropriately modified inhomogeneous boundary conditions

$$\nabla^2\chi=0:\quad \chi \text{ given,}$$

or

$$\nabla^2\chi=0:\quad \frac{\partial\chi}{\partial\phi} \text{ given.}$$

These represent the solution of the potential flow problem on a sphere due to imposed flow at the equatorial boundary.

Extending a result of potential flow theory (e.g., Batchelor, 1967, p. 385) to the spherical case, it is easy to show that

$$\frac{1}{a}\frac{\partial\chi}{\partial\phi}=v,\qquad \frac{1}{a}\frac{\partial\chi}{\partial\lambda}=u\cos\phi,$$

must both be bounded by their values on the equatorial boundaries.

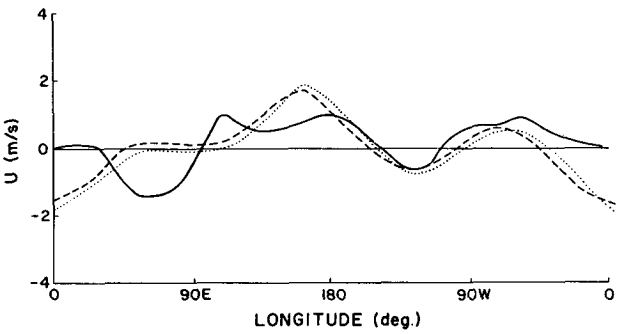

FIG. A1. 200 mb divergent zonal wind component, averaged from the equator to 30°N. The solid curve is Krishnamurti's result as in Fig. 9. Dashed and dotted curves are diagnosed from the non-elliptic pressure fields, wavenumbers 1, 2, 3, using $\chi=0$ and Krishnamurti's χ values, respectively, as equatorial boundary conditions.

The interior zonal flow might be most sensitive to boundary changes because of the $\cos\phi$ factor and because it is relatively weaker (compare Figs. 9 and 10). Fig. A1 demonstrates that the zonal flow in the latitude belt extending from the equator to 30°N is changed very little by using Krishnamurti's (1971) χ variation on the equator instead of homogeneous values.

We have also solved the Neumann problem using Krishnamurti's (1971) zonally averaged v of -0.5 m s^{-1}. This test (which also dictates that partial convergent compensation occurs in the Southern Hemisphere) has more impact upon the diagnosed value of u in the tropical belt (Fig. A2). The amplitude is increased by a factor of 2, but the phase is quite similar to the other cases.

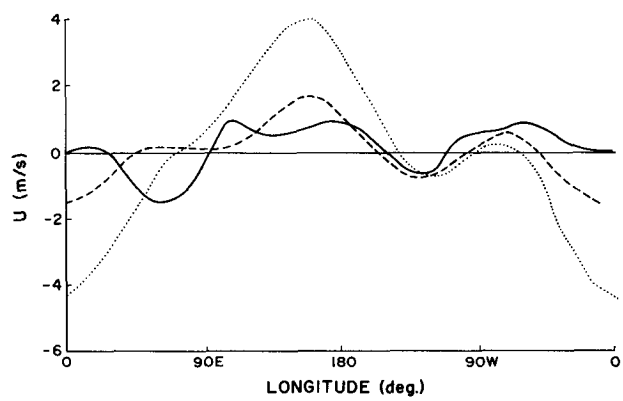

FIG. A2. As in Fig. A-1 except that the dotted curve represents diagnoses specifying $a^{-1}\partial\chi/\partial\phi=-0.5$ m s^{-1} as the equatorial boundary conditions.

These tests, and several others, confirm that the general conclusions of Section 3 are not materially affected by reasonable variation of boundary conditions and convergent compensation. The long waves contain most of the divergent flow variance, the magnitude of which is generally larger than observed. The most serious phase discrepancy occurs in the zonal flow in a 60° longitude interval centered on the Greenwich meridian. Here our diagnoses produce strong easterly flow, while Krishnamurti *et al.* (1973) observe weak westerlies for the year 1967. However, in another observational study for 1972 easterly flow is observed over much of this region (Krishnamurti *et al.*, 1975).

REFERENCES

Adams, J. C., A. K. Cline, M. A. Drake and R. A. Sweet, 1975: *Partial Differential Equations, PWSSP*. NCAR software support library, Vol. 2. NCAR Tech. Note TN/IA-105, 141–157.

Batchelor, G. K., 1967: *An Introduction to Fluid Dynamics*. Cambridge University Press, 614 pp.

Charney, J. G., 1955: The use of the primitive equations of motion in numerical prediction. *Tellus*, **7**, 22–26.

Cressman, G. P., 1959: An operational objective analysis system. *Mon. Wea. Rev.*, **87**, 367–374.

Ellsaesser, H. W., 1968: Comparative test of wind laws for numerical weather prediction. *Mon. Wea. Rev.*, **96**, 277–285.

Houghton, D. D., 1968: Derivation of the elliptic condition for the balance equation in spherical coordinates. *J. Atmos. Sci.*, **25**, 927–928.

——, D. P. Baumhefner and W. M. Washington, 1971: On global initialization of the primitive equations: Part II. The divergent component of the horizontal wind. *J. Appl. Meteor.*, **10**, 626–639.

Jenne, R. L., 1975: Data sets for meteorological research. NCAR Tech. Note TN/IA-111, 172 pp.

Krishnamurti, T. N., 1971: Observational study of the tropical upper tropospheric motion field during the Northern Hemisphere summer. *J. Appl. Meteor.*, **10**, 1066–1096.

——, E. G. Astling, M. Kanamitsu, 1975: Two-hundred mb wind field June, July, August 1972. Report, Department of Meteorology, Florida State University, 115 pp.

——, M. Kanamitsu, W. J. Koss and J. D. Lee, 1973: Tropical east-west circulation during the northern winter. *J. Atmos. Sci.*, **30**, 780–787.

MacDonald, A. E., 1976: On a type of strongly divergent balanced flow. *Mon. Wea. Rev.* (in press).

McDonnell, J., 1962: On the objective analysis system used at the National Meteorological Center. Tech. Memo. No. 23, National Meteorological Center, Suitland, Md., 31 pp.

——, 1967: A summary of first guess fields used for operational analyses. Tech. Memo. No. 38, National Meteorological Center, Suitland, Md., 17 pp.

Miyakoda, K., 1956: On a method of solving the balance equation. *J. Meteor. Soc. Japan*, **34**, 364–367.

Paegle, J., and J. N. Paegle, 1974: An efficient and accurate approximation of the balance wind with application to non-elliptic data. *Mon. Wea. Rev.*, **102**, 838–846.

——, and ——, 1976: On the realizability of strongly divergent supergradient flows. *J. Atmos. Sci.* (in press).

Sadler, J. C., 1975: The upper tropospheric circulation over the global tropics. Hawaii Institute of Geophysics, University of Hawaii, UHMET-75-05, 35 pp.

Shuman, F. G., 1957: Numerical methods in weather prediction: I. The balance equation. *Mon. Wea. Rev.*, **85**, 329–332.

Washington, W. M., and D. P. Baumhefner, 1975: A method of removing Lamb waves from initial data for primitive equation models. *J. Appl. Meteor.*, **14**, 114–119.